Prediction of Relative Permeability and Capillary Pressure using Digital Rock Physics: Case Study on two Giant Middle Eastern Carbonate Reservoirs.

Kamel Zahaf[1], Thierry F. Lecoq[1], Badar S. AL Badi[1], Sven Roth.[2], Hu Dong[2] and Martin J. Blunt[2,3]

[1]ADMA-OPCO [2]iRock Technologies [3]Imperial College London

ABSTRACT

Carbonate reservoir rocks are often highly complex, exhibiting extreme heterogeneity in the size, shape, connectivity and wettability of the pore space. In turn this variability strongly impacts the behavior of the capillary pressure and relative permeability and hence the oil recovery. Special core analysis cannot describe or separate these effects since the measurements are limited in the number of samples that can be handled, as well as the displacement cycles and wettabilities that can be considered.

We study 16 samples from two large Middle Eastern carbonate reservoirs (both limestones and dolomites). Static and dynamic properties of these rocks were determined through a combination of nano to cm scale sample selection and imaging to capture micro-porosity, macro-porosity and vugs, and multi-scale generalized network modeling and upscaling to capture the four orders of magnitude variation in pore size. The pore-scale distribution of contact angle was tuned to match one set of waterflood capillary pressure curves, which indicated mixed-wet characteristics with a tendency to be weakly oil-wet. On benchmark samples, the measured waterflood relative permeability was compared successfully to the predicted results.

Samples with the widest range of connected pore sizes – principally the limestones with a mix of micro-, macro- and vuggy-porosity – tended to display oil-wet type waterflood behavior, implying poor recovery, whereas the dolomite samples with a more restricted range of pore size showed mixed-wet characteristics in their flow response with more favorable recoveries. This study shows the value of digital rock technology, which aids the identification of multiphase flow rock types and quantifies how the pore size distribution, connectivity, mineralogy and wettability impact local displacement efficiency.

INTRODUCTION

Digital Rock Physics (DRP) or pore-scale modeling has received considerable attention in recent years as a complimentary and integral technology to laboratory measurement for the prediction of reservoir properties, for which the right laboratory measurements are difficult to perform or require long measurement times [1].

In network modeling the void space of a rock is represented at the microscopic scale. The topology of the pore space is determined using the maximal ball algorithm to extract

pore networks from macro- and microporosity [2]. The network extraction algorithm outputs a robust network suitable for computation of multiphase fluid displacement.

Multiphase flow properties are simulated based on the pore-scale modeling technology pioneered by Imperial College and adopted by iRock Technologies [3]. The displacement of one phase by another is computed semi-analytically on the pore space, using expressions for threshold capillary pressures derived for different pore and throat shapes and sizes. Contact angles are assigned to the network elements to reproduce any available wettability measurements. A multi-scale approach is employed, where networks are generated from images of different resolution and then combined and upscaled to make predictions for the full core.

DIGITAL ROCK PHYSICS (DRP) WORKFLOW

Step I: Core selection and characterization

Core characterization involved visual description, plug overview X-ray scanning, **E**valuation of **M**inerals, **SCAN**ning electron microscopy (**QEMSCAN**), Backscattered Electrons, (BSE) derived porosity and pore-size distribution. All this information lead to the micro-CT and nano-CT subsampling plan. Heterogeneity and variability in the sample plug will dictate the strategy of sampling.

Step II: Rock model construction

Prior to any simulations, the 3D X-ray images were processed and segmented. The processing includes image enhancement (noise reduction) and cropping the volume into a three-dimensional rock model. A quality control at this step is needed to validate pore size distribution and porosity of the digital rock model with laboratory data before proceeding with data acquisition, described later. Once the model is validated, rock properties are then calculated.

Step III: Upscaling and multiphase flow modeling

The goal of upscaling is to average properties from pore-scale network modeling to the whole core plug, where different regions may have different properties.

The imaging of rock samples and upscaling of the results are performed using a proprietary three-stage approach [2]. The basis of the method is to construct a generalized network model of the rock rather than being an explicit representation of large "pores" connected by "throats" as in traditional pore-network modelling approaches, we instead consider interconnected elements. These elements may indeed be real pores and throats, or could represent an averaged behavior of a region of micro-porosity. In this way we can construct a network at any scale, representing features spanning many orders of magnitude in scale. The wettability constrained to SCAL data is obtained from the lab to predict waterflood capillary pressure and relative permeability.

ROCK CHARACTERIZATION

Carbonate reservoirs are complex in their structure and pore geometries, and often display heterogeneity at all length scales [4], as is the case in this study. Core samples from two

Middle Eastern offshore carbonate fields A and B were used in this study. Table 1 below provides a summary of the 16 samples. Dolomitic and calcitic samples were carefully selected covering wide permeability and pore-type ranges.

Table 1. Core description and summary results.

WELL	Plug_No	Plug description	DRP φ total	DRP K (mD)	CCA_Lab φ total	CCA_Lab K (mD)
A	3	Biomoldic dolostone, the darker anhydrite patches are scattered within the lighter dolomite matrix; visible pores are only present in the dolomite material. Two recrystallized fractures roughly parallel to each other are observed	0.1771	1	0.178	4
A	15	Dolostone, part of the core is more vuggy then the other parts, but there is no apparent 'bedding'. Some mm- to cm-scale anhydrite patches are observed	0.216	185	0.23	228
A	18	Dolomudstone, the rock is homogeneous, and has a fine-grained texture. There are few visible pores. The sample has small breaks filled with epoxy.	0.2798	72	0.304	73
A	19	Dolomudstone, the sample is oil stained and black in color. The rock appears homogeneous, and has a fine texture.	0.2083	15	0.2283	22
A	23	Dolomudstone, homogenous with visible vugs. A set of recrystallized fractures (dark lines) roughly parallel to the long axis of the core plug are observed.	0.1743	45	0.176	56
A	30	Dolomudstone, visible pores are up to ~0.5-1 mm in diameter. The sample has a strong oil smell. The cutting surface after core cleaning shows subtle layering/burrows	0.2038	58	0.214	50
A	33	Dolomudstone, the rock is characterized by alternating porous (vugs up to ~1 mm) 'layers' and cemented 'layers' showing no visible pores.	0.1809	70	0.18	58
A	40	Vuggy, bioclastic packstone, vugs up to ~1 mm in diameter; the sample contains abundant bioclasts and anhydrite patches. Some large vugs are associated with anhydrite dissolution.	0.2084	55	0.2059	68
A	48	Mud-dominated packstone, abundant vugs up to ~1 mm in diameter; the sample contains abundant bioclasts, primarily algal, foram, and bivalve in origin.	0.2098	26	0.21	25
A	113H	Dolostone, the rock is relatively homogeneous with primarily intercrystalline pores. Abundant calcite cement and anhydrite patches are scattered in the rock sample	0.173	306	0.176	347
A	127H	Dolostone, the rock show abundant vugs that are up to 0.5-1 mm in diameter and are unevenly distributed (no apparent bedding). Some anhydrite patches are observed.	0.2754	677	0.28	524
B	8	Wackestone, the rock contains abundant bioclasts (primarily foram) and large vugs up to several mm in diameter	0.2887	37	0.291	45
B	69	Wackestone, fossiliferous with shell fragments up to ~5 mm long, abundant vugs up to ~0.5 mm in diameter.	0.2935	4.7	0.289	11.5
B	291	Mud-dominated packstone, abundant vugs that are up to 0.5-1 mm in diameter. There are a few clasts (with the largest one ~12×7 mm) that can be observed on core plug surface.	0.1664	13	0.159	15
B	329	Dolomudstone, the rock is relative homogeneous, and has a fine texture. A fracture (mechanical in nature) cuts through one end of the core plug obliquely.	0.2059	17	0.202	12.9
B	351	Packstone, the rock has abundant vugs that are up to ~1 mm in diameter. There are a few holes/breaks on the core plug surface that were filled with epoxy	0.2079	20	0.215	29

All the plugs were imaged; see Figure **1**, with a voxel size of approximately 40 μm. This overview scan provided information about the heterogeneity of the core plug and served as the sample volume to upscale all properties acquired at the pore scale.
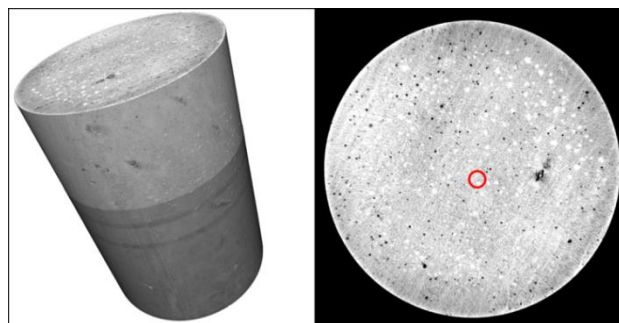
Figure 1. Plug MCT images and plug heterogeneity assessment (sample A_19).

Figure 2 shows a high-resolution BSE mosaic image**.** BSE mosaics are images of a large area at nanometer resolution, acquired with a scanning electron microscope. Two sets of images were taken per sample: one overview image of the entire plug surface with a pixel size of 488 nm, and additional representative sub-areas of approximately 2×2 mm imaged

at a pixel size of 48.8 nm. The resulting images were used to extract pore-size distributions (from nm to cm) to characterize the pore space of the samples and to quality control the MICP and NMR measurements.

Large area BSE image. Image dimension
15.0 x 16.3 mm; pixel size is 488 nm.

Sub-area BSE image. Image dimension
2.2 x 2.1 mm; pixel size is 48.8 nm.
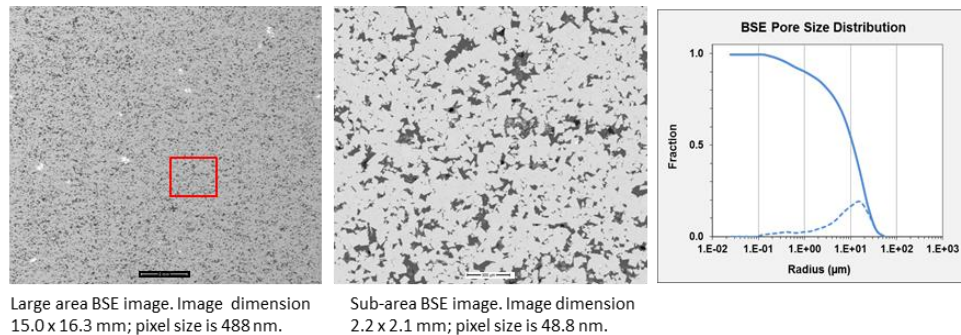
Figure 2. BSE images and BSE-derived pore size distribution.

The overview micro-CT, QEMSCAN and BSE images data were used to construct a sub-sampling strategy. As carbonate reservoirs are very complex, sub-sample strategy may differ from sample to sample in number and resolution.

POROSITY AND PERMEABILITY PREDICTIONS

Pore system analysis and permeability for the 11 samples from well A are summarized in Table 1. Seven of them are pure dolomitic, two are dolomite-dominated but contain different amounts of calcite nodules (sample A_15: 90% dolomite/7% calcite; sample A_113H: 80% dolomite/20% calcite). Two other samples are primarily calcitic with admixture of dolomite (A-40 and A_48).

Three of the samples were high permeability (k > 100 mD) with no microporosity and some vugs (samples A_113H, A_127H and A_15). Three other samples also contained no micro-porosity, but overall had smaller, less well-connected pores with permeability in the range 15-72 mD: samples A_18, A_19 Figure 2 and A_23. The remaining five samples contained microporosity with lower permeabilities from 26 –70 mD with one sample, A_3, with a much lower predicted permeability of 1 mD.

Five samples from well B (Table 1) were investigated. All samples are calcitic, except for the dolosiltstone sample B_329, which contains a mineral mixture of 75% dolomite and 25% calcite. Dolomite builds the framework of this rock, while microcrystalline calcite minerals occupy and reduce the pore space. The samples have intermediate permeability in the range 4.7 –37 mD. Two samples contain only macro-porosity and some vugs: B_291 and B_329. The lowest permeability sample is almost all micro-pores, the mud-to wackestone B_69. The remaining two samples (wackestone B_8 and packstone B_351).

Figure 3 shows the porosity partitioning for four samples. Limestone samples are made of micro-macro and vuggy porosity, while the dolomites have more restricted range of pore size. At this stage, it is important to understand the rock architecture of the pore system and thus the connectivity between them. Later we will show the impact on the

multiphase flow behavior and recovery. Figure 3 shows that the DRP predictions of porosity and permeability compare well with the measurements, Table 1.
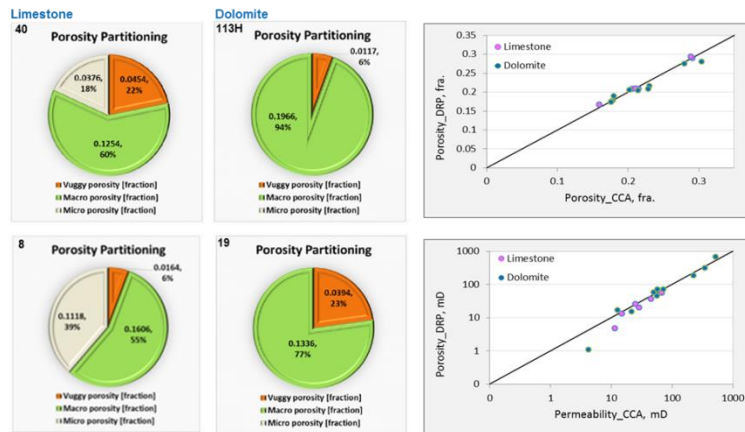
Figure 3. (a) Porosity partitioning based on image segmentation (b) Porosity and permeability predictions against laboratory measurements.

PORE THROAT DISTRIBUTION (MICP) CALIBRATION

The objective of this step is to calibrate the 3D pore networks using trim MICP. First, the pore throat distribution was derived from DRP then compared blindly to the MICP results (Figure 4). Where there are discrepancies, different sub-volumes were selected to produce DRP models to capture the small-scale heterogeneity and upscaled to provide a better match to the data. In summary, a realistic network topology combined with network properties tuned to experimental data such as MICP is sufficient to predict single and multiphase properties.
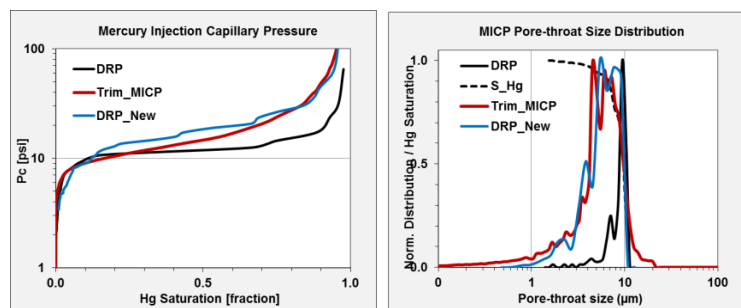
Figure 4. Sample A_15: Mercury injection capillary pressure (left) and pore throat distribution (right) comparison before and after updating to capture small-scale heterogeneity.

SIMULATION OF WATERFLOODING
Capillary pressure prediction

The up-scaled simulated primary drainage capillary pressure was compared with the measured laboratory data, see Figure 5. The contact angles in the simulations were adjusted to match the laboratory waterflood capillary pressure measured on one sample (A-30). In this case, we assume a weakly oil-wet condition with around 60% of the pore space oil-wet with an average contact angle of 135°.
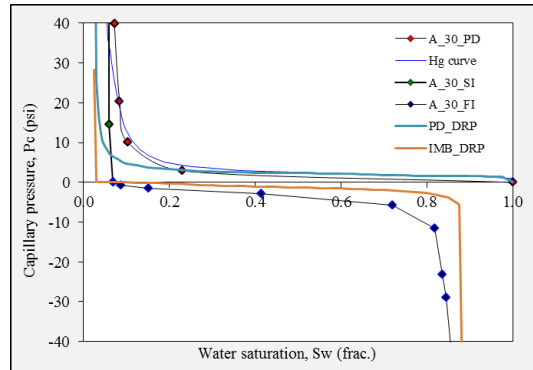
Figure 5. Sample A_30-Comparison of the measured primary drainage and imbibition capillary pressure.

Primary drainage relative permeability prediction

Figure 6 shows the predicted primary drainage relative permeability for both dolomite and limestone samples. In general, dolomite samples with a unimodal pore-size distribution (for instance, sample B_329, Figure 7) have a poor connectivity of the oil phase. In contrast, the limestone samples have a more connected pore system with higher oil relative permeabilities (for instance, sample B_351, Figure 7).
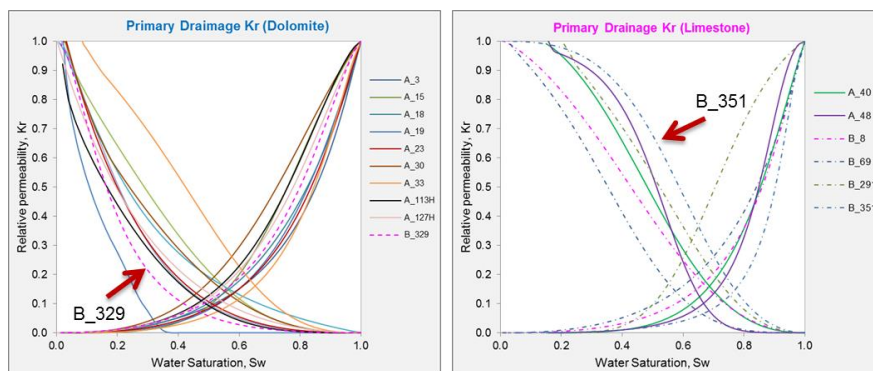
Figure 6. Primary Drainage relative permeability: dolomite (left) and limestone (right).
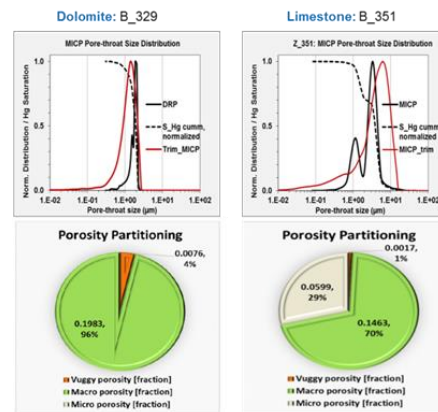
Figure 7. Pore throat distribution and porosity portioning showing the impact of pore type distribution on primary drainage relative permeability.

Prediction of waterflood relative permeability

The principal control on waterflood relative permeability is the connectivity of the phases in the pore space, governed by wettability (the contact angles) and pore structure. A rough indicator of waterflood recovery efficiency is not necessarily the theoretical residual saturation, but the water saturation where the oil and water relative permeability curves cross –the higher the value, the better the likely local recovery from waterflooding. Figure 8 compares the predicted and measured waterflood relative permeability curves for two samples B_69 (limestone) and A_19 (dolomite).

1- Overall the shape of the predicted relative permeability, particularly the oil relative permeability, is captured compared to the measured laboratory relative permeability which means the overall pore type system is well captured in the 3D pore network.
2- The predicted water relative permeability end point did not match the measured data: this could be due either to a poor characterization of wettability, or the true end-point not being measured in the experiments.

Figure 9 shows the predicted waterflood relative permeability for all the samples. We see two types of behaviour: classical oil-wet for the limestone samples (with the corss-over saturation marked by the red arrow) and mixed –wet for the dolomite samples (green arrow).

Oil-wet type behavior
For the limestone*s*, the saturation at which the waterflood relative permeability curves cross is less than 0.5, implying poor recovery. The oil relative permeability is lower for waterflooding than for primary drainage, as the oil now fills the smaller pores, while water in the larger pores, and has a higher relative permeability. This behavior is also seen for cores taken from the giant Ghawar field in Saudia Arabia [5]. Our samples have a mix of micro, macro and vuggy porosity with a very high oil relative permeability in primary

drainage, Figure 6. This implies that there is a well-connected pathway of larger pores: these, largely oil-wet regions fill with water during waterflooding, leading to high water relative permeabilities, extreme relative permeability hysteresis, early water breakthrough and poor recoveries.
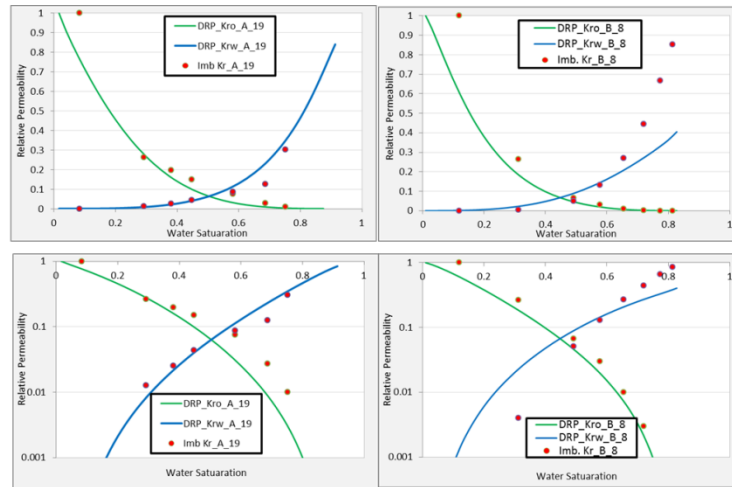
Figure 8. Waterflood relative permeability, comparing measured (points) and predicted (lines) data: and dolomite (left, A_19) and limestone (right, B_8)
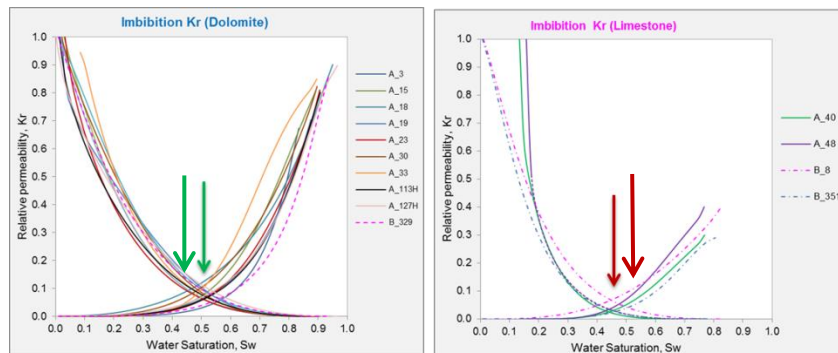
Figure 9. Waterflood relative permeability; dolomite (left) and limestone (right). The arrows indicate the cross-over saturation which is a guide to recovery: green is favorable while red is less favorable.

Mixed-wet type behavior

For the dolomites, we see higher cross-over saturations and very low waterflood water relative permeability, implying that during waterflooding the water can have a low connectivity at low saturation as there is no clear path of large oil-wet pores through the samples. This behavior has been seen experimentally from other cores from Abu Dhabi [6]. For samples A_113H, A_117H, A_19 and A_23, we see a cross-over saturation of greater than 0.5 and waterflood water relative permeabilities that can lie below those for primary drainage. In the wettability sensitivities and scanning curves, optimal recovery is generally for a mixed-wet, or at least not completely oil-wet state, and for intermediate

initial saturations, where the connectivity of the water is most restricted. These samples tend to have the highest permeability with a well-connected pore space, but without huge extremes in pore size and no micro-porosity. It is not possible for the water to occupy a preferential channel of much larger pores during waterflooding.

CONCLUSIONS

- A realistic multi-scale network topology with properties tuned to experimental data allows a robust prediction of multiphase flow properties.
- The DRP models were able to match measured relative permeability data.
- This analysis allowed the interpretation of the flow behavior and local displacement efficiency. Dolomites with a relatively narrow range of pore size gave favorable waterflood recoveries under mixed-wet or weakly oil-wet conditions. This is because – at the pore scale – the water remains poorly connected during waterflooding. In contrast the limestones, with a wider range of pore size and a pathway of connected larger pores displayed extreme relative permeability hysteresis between primary drainage and waterflooding with high water relative permeability during waterflooding. Here water rapidly connects across the pore space, leading to unfavorable local displacement.
- DRP is a useful complement to SCAL and enables the confident and robust assignment of rock types based on multiphase flow and recovery characteristics.
- Future work could extend this study, and use *in situ* measurements of contact angle to assign wettability.

ACKNOWLEDGMENTS

REFERENCES

1. Masalmeh, X. K., X. Jing, S. Roth, C. Wang, H. Dong, "Towards Predicting Multi-Phase Flow in Porous Media Using Digital Rock Physics: Workflow to Test the Predictive Capability of Pore-Scale Modeling" *SPE*-177572-MS (2015).
2. Dong H. and M. J. Blunt, "Pore-network extraction from micro-computerized-tomography images" *Physical Review E*, (2009), **80**, 3, 036307.
3. Valvatne, P.H. and Blunt, M.J, "Predictive Pore Scale-Modeling of two-phase flow in mixed-wet media", *Water Resources Research*, (2004), **40**, W07406, doi: 10.1029/2003WR002627.
4. Natarajan D., Naveen K., Verma T., Abdul Salam, and Ibrahim Al Sammak, Kuwait Oil Co; Koronfol S., Dernaika M., The WJ. 'Computation of Relative Permeability Curves in Middle Eastern Carbonates Usung Digital Rock Physiscs" IPTC-18211-MS (2014).
5. Okasha, T. M., J. J. Funk, and Rashidi, H. 2007. Fifty years of wettability measurements in the Arab-D carbonate reservoir. In: SPE 105114, proceedings of the SPE Middle East Oil and Gas Show and Conference, Manama, Kingdom of Bahrain.
6. Dernaika, M. R., Basioni, M. A., Dawoud, A. M., Kalam, M. Z., and Skjaeveland, S. M. 2013. Variations in Bounding and Scanning Relative Permeability Curves With Different Carbonate Rock Type. SPE Reservoir Evaluation & Engineering, 16(3), 265-280.